Mutant MYO1F alters the mitochondrial network and induces tumor proliferation in thyroid cancer

Mutant MYO1F alters the mitochondrial network and induces tumor proliferation in thyroid cancer

Chiara Diquigiovanni[1], Christian Bergamini[2], Cecilia Evangelisti[3], Federica Isidori[1], Andrea Vettori[4], Natascia Tiso[4], Francesco Argenton[4], Anna Costanzini[1,2], Luisa Iommarini[2], Hima Anbunathan[5], Uberto Pagotto[1], Andrea Repaci[6], Giulia Babbi[2], Rita Casadio[2], Giorgio Lenaz[3], Kerry J. Rhoden[1], Anna Maria Porcelli[2], Romana Fato[2], Anne Bowcock[5], Marco Seri[1*], Giovanni Romeo[1], Elena Bonora[1*]

[1]Department of Medical and Surgical Sciences, DIMEC, St. Orsola-Malpighi Hospital, University of Bologna, Bologna, Italy.

[2]Department of Pharmacy and Biotechnology, FABIT, University of Bologna, Bologna, Italy.

[3]Department of Biomedical and Neuromotor Sciences, DIBINEM, University of Bologna, Bologna, Italy.

[4]Department of Biology, University of Padova, Padova, Italy

[5]National Heart and Lung Institute, Imperial College, London, United Kingdom.

[6]Endocrinology Unit, St. Orsola-Malpighi Hospital, Bologna, Italy.

Running Title: ***MYO1F in thyroid cancer***

Keywords: Non-Medullary Thyroid Carcinoma; TCO locus; whole exome sequencing; MYO1F; mitochondrial network

All authors declare no conflict of interests

Financial support: The work was supported by AIRC grant IG2015-17069 to M.S., Italian Ministry of Health grants GR-2012 “DIANE” to E.B, RF-2011-02350857 to KJR, and EU FP7 Marie Curie project MEET-317433 to AMP.

*To whom correspondence should be addressed: Prof. Marco Seri, Unit of Medical Genetics, Department of Medical and Surgical Sciences, St. Orsola-Malpighi Hospital, University of Bologna, 40138 Bologna, Italy. Telephone: +390512088421; fax: +390512088416; email: marco.seri@unibo.it.

Dr. Elena Bonora, Unit of Medical Genetics, Department of Medical and Surgical Sciences, St. Orsola-Malpighi Hospital, University of Bologna, 40138 Bologna, Italy. Telephone: +390512088434; fax: +390512088416; email: elena.bonora6@unibo.it.

Novelty and Impact Statements

We report the identification of the mutation at the thyroid cancer predisposing locus on chromosome 19p13.2, in the gene *MYO1F*. Cell models carrying mutant MYO1F have a significant advantage in colony formation, invasion, anchorage independent growth, and show an altered mitochondrial phenotype similar to the one observed in the patients' tumors. Our study indicates for the first time that MYO1F has a role in thyroid cancer predisposition.

Abstract

Familial aggregation is a significant risk factor for the development of thyroid cancer and Familial Non-Medullary Thyroid Cancer (FNMTC) accounts for 5-7% of all NMTC. Whole Exome Sequencing analysis in the family affected by FNMTC with oncocytic features where our group previously identified a predisposing locus on chromosome 19p13.2, revealed a novel heterozygous mutation (c.400G>A, NM_012335; p.134G >S) in exon 5 of *MYO1F*, mapping to the linkage locus. In the thyroid FRTL-5 cell model stably expressing the mutant MYO1F p.134G>S protein we observed an altered mitochondrial network, with increased mitochondrial mass and a significant increase of both intracellular and extracellular Reactive Oxygen Species, compared to cells expressing the wild-type protein or carrying the empty vector. The mutation conferred a significant advantage in colony formation, invasion and anchorage independent growth. These data were corroborated by *in vivo* studies in zebrafish, since we demonstrated that the mutant MYO1F p.134G>S, when overexpressed, can induce proliferation in whole vertebrate embryos, compared to the wild-type one. *MYO1F* screening in additional 192 FNMTC families identified another variant in exon 7, which leads to exon skipping, and is predicted to alter the ATP-binding domain in MYO1F. Our study identified for the first time a role for *MYO1F* in NMTC.

Introduction

Familial aggregation is a significant risk factor for the development of thyroid cancer derived from follicular epithelial cells (Non-Medullary Thyroid Carcinoma, NMTC). When the primary cancer site is considered, the thyroid gland shows the highest estimate of familial relative risk among all organs (5-10 fold compared to 1.8 and 2.7 for breast and colon cancer, respectively) [1]. Familial NMTC (FNMTC) accounts for 5-7% of all NMTC, although some cases occur in the context of familial syndromes such as Cowden disease (CS). CS syndrome is caused by germline mutations in PTEN [2] and in genes encoding the different subunits of succinate dehydrogenase (SDHB-D) [3]. However, the genetic alterations underlying the vast majority of non syndromic cases are unknown. The recognition of familiarity is critical for early diagnosis and treatment of the disease, since these patients present more aggressive tumors that are less likely to respond to current therapies and have a worse outcome [4]. A search for susceptibility genes, undertaken using linkage-based approaches, led to the identification of several predisposing loci on chromosomes 14q31, 19p13.2, 2q21, and 1q21 [5, 6]. Causative mutations were identified at the 14q31 locus in the *DICER1* gene, which encodes for an enzyme required for miRNA maturation [7]. A predisposing locus for FNMTC was previously identified on chromosome 19p13.2 in a multigenerational family with multiple individuals affected by thyroid carcinoma with oncocytic features (oxyphilia; TCO), with autosomal dominant inheritance [8]. In the present study, we report Whole Exome Sequencing (WES) data, mutation screening and functional studies providing evidence that germline mutations in *MYO1F*, including the one found in the TCO pedigree on chromosome 19p13.2, lead to NMTC.

Materials and Methods

The study was approved by the committee for protection of persons in biomedical research of Lyon (CCPRB A-96.18) and by the IARC Ethical Review Board (Project 95-050, amendment 01-013). Informed consent was obtained by clinicians, in each collaborating center.

Subjects

The TCO family has been previously reported [8] and the main clinical characteristics are reported in the Supporting Data file. PTCs were diagnosed in individuals II-5, III- 3, and III-7 at the ages of 41, 27, and 11 years, respectively. 192 FNMTC patients included in the mutation screening came from the families collected between 1996 and 2012 through the International Consortium for the Genetics of Non-Medullary Thyroid Carcinoma. 149 female patients and 43 males were included (age of onset: 11-84 yrs, mean age=42), thyroid cancer diagnosis as reported in Table S1.

WES analysis

WES was performed on three individuals from the TCO family, two affected by thyroid carcinoma with oncocytic features (individuals II-3; III-7, Figure 1A) and one affected by adenoma (II-4), according to the pipeline reported in the Supporting Data file. Variants were confirmed by PCR and direct sequencing.

Cell lines

The FRTL-5 cell line is a stable thyroid cell line derived from normal thyroid glands from 5 to 6-week-old Fisher rats [9]. All cells were cultured in 6H5 medium consisting of Coon's modified Ham's F12 medium (Sigma-Aldrich, St. Louis, MO, USA) supplemented with 5% newborn calf serum (NCS) (Sigma-Aldrich), 1 μg/ml insulin, 10 nM hydrocortisone, 5 μg/ml apo-transferrin, 10 ng/ml gly-his-lys, 10 ng/ml somatostatin, 1 mU/ml TSH (Sigma-Aldrich, St. Louis, MO, USA) and

penicillin/streptomycin (EuroClone, Milan, Italy). Cells were propagated in a fully humidified atmosphere of 5% CO_2 at 37°C.

COS7 cells derived from monkey kidney tissue were grown in DMEM, 10% fetal bovine serum, 2 mM L-glutamine, 100 U/ ml penicillin and 100 μg/ml streptomycin, in a humidified incubator at 37°C with 5% CO_2.

pCMV6-MYO1F p.134 G>S plasmid generation via site-directed mutagenesis

The construct pCMV6 encoding wild-type *MYO1F* (RC207069) was purchased from OriGene (OriGene Technologies, Rockville, MD, USA) in frame with the tag DDK and containing neomycin resistance (G418) for stable selection. The mutation c.400G>A was inserted using the Q5 Site-direct Mutagenesis kit, according to the manufacturer's instruction (New England Biolabs, Ipswich, MA, USA) using the oligonucleotides forward 5′-AGGTGTCTGGCGGAAGCGAGAAGGTCCAG-3′ and reverse 5′-TGGAGATGTAGCCCATGATTATTTGGCT-3′. The site-directed mutagenesis was verified by plasmid direct sequencing.

Generation of FRTL-5-stably transfected cell lines

7.5 μg of pCMV6 empty, pCMV6-MYO1F-wt and pCMV6-MYO1F-G134S plasmids were transfected using liposomes according to the manufacturer's instructions (Lipofectamine 2000, ThermoFisher Scientific, Grand Island, NY, USA). 48 hours after transfection, selection was obtained by supplementing complete medium with 500 μg/ml G418 (ThermoFisher Scientific) for 2 weeks. Isolated clones were grown with 200 μg/ml G418.

Western blot

A detailed protocol is reported in the Supporting Information, including the list of primary antibodies used.

Plate colony formation assay

$2.5x10^4$ cells were seeded in duplicate and incubated for 20 days at 37°C. Cells were washed in PBS and fixed with cold Trichloroacetic acid (TCA) 50% at 4°C for 1h, then TCA was eliminated and cells were dried at room temperature for 16 hours. Cells were stained with SRB 0.4% in 1% acetic acid for 30 min, washed with 1% acetic acid 4 times and photographed with ChemiDoc™ XRS+ (Biorad). Area and number of colonies were quantified with the *ImageJ* software (National Institute of Health, Bethesda, MD, USA) discarding colonies <1 pixel.

Soft agar colony assay

Stable cell lines were seeded in triplicate in a 0.48% top agar in growth medium over a layer of 0.8% agar in a 6-well plate at a density of $1x10^5$ cells/ml. Plates were incubated at 37°C and 5% CO_2 for 12 days, monitoring for colony formation. Medium was replaced every 5 days. After 12 days, colonies were photographed and analyzed with *ImageJ* software.

Wound healing assay

Stable cell lines were plated onto six-well plates and allowed to form a confluent monolayer. The cell monolayer was then scratched in a straight line to make a 'scratch wound' with a 10-µl tip and the cell debris was removed by washing the cells with phosphate-buffered saline. 6H5 medium supplemented with 10% NCS and 200 µg/ml of neomycin was added, and images of the closure of the scratch were captured at 0 and 7 days. Images were analyzed with the *TScratch* software [10].

Iodide transport

Iodide uptake by FRTL-5 cells was measured by live cell imaging with the fluorescent halide biosensor YFP-H148Q/I15L, as previously described [11, 12].

Mitochondrial morphology and mass assessment via live cell imaging

Mitochondrial morphology was assessed by live imaging, using a Nikon Eclipse 80 microscope (Nikon, Tokio, Japan) according to [13]. Circularity measurements were collected using *ImageJ* standard tools.

Mitochondrial mass measurements

$1x10^4$ FRTL-5-stable cell lines were seeded in quadruplicate in 96-well culture plates. The next day, cells were loaded with 50 nM MTG for 30 minutes at 37°C in complete medium. After washing twice with medium, MTG fluorescence was recorded in a plate reader (EnSpire, PerkinElmer). MTG fluorescence values were expressed as RFU/viable cells. Cell viability was assessed with a resazurin-based method.

Mitochondrial potential measurement via JC-1

The fluorescent probe JC-1 (5, 5′ ,6, 6′ -tetrachloro-1, 1′ , 3, 3′ -tetraethylbenzimidazol carbocyanine iodide) was used to measure the mitochondrial membrane potential ($\Delta\phi$), as described in the Supporting Data.

Cellular respiration

Oxygen consumption in intact cells

$\sim 1.5x10^6$ FRL5-stable cell lines were harvested at 70-80% confluence, washed in PBS, re-suspended in complete medium and assayed for oxygen consumption at 30°C using a thermostatically controlled oxygraph chamber (Instech Mod. 203, Plymouth Meeting, PA, USA). Basal respiration was measured in their respective media and compared with the one obtained after injection of oligomycin (1 μM) and FCCP (1–6 μM). Antimycin A (5 μM) was added at the end of experiments to completely block the mitochondrial respiration. Data were normalized to protein content determined by the Lowry method.

ROS quantification

Intracellular ROS

FRTL-5-stable cell lines were seeded at $5x10^4$ cells/well and incubated 16 hours. Cells were treated with 10 μM DCFDA dissolved in medium for 1 hour. Then, cells were washed twice with PBS and incubated for 12 hours in complete medium. Finally, cells were washed with PBS and the fluorescence emission from each well was measured (λexc = 485 nm; λem = 535 nm) with a multi-plate reader (Enspire, Perkin Elmer). Data are reported as the mean ± standard deviation of at least three independent experiments.

Extracellular ROS

FRTL-5-stable cell lines were seeded at $5x10^4$ cells/well and incubated 16 hours. Cells were treated with 10 μM Amplex red (N-acetyl-3,7-dihydroxyphenoxazine), 0.025 U/ml HRP (horseradish peroxidase) dissolved in complete medium for 16 hours. The medium was collected and measured (λexc 530, λem 590) with a multiplate reader (Enspire, Perkin Elmer). Data were normalized for cell number using resazuring assay. Data are reported as the mean ± standard deviation of at least three independent experiments.

In vivo study of mutant MYO1F

Zebrafish embryos and adults were maintained and mated according to standard procedures. Mutant and wild-type capped *MYO1F* mRNAs were synthesized with the SP6 mMESSAGE mMACHINE kit (Ambion, ThermoFisher Scientific) using as template the PCS2+MYO1F-G134S and PCS2+MYO1F-wt plasmids respectively. Wild-type zebrafish embryos were injected at one-cell stage with 150 pg of MYO1F-wt or MYO1F-G134S mRNA and then fixed at 48 hpf. To determine the cell proliferation patterns, a whole-mount immunostaining with the anti-phospho-Histone H3 (pH3) antibody (Millipore, Darmstadt, Germany) was performed. We counted the mitotic cells along the trunk of each fish (from the yolk extension to the tip of the tail)

and calculated the average number of pH3 positive cells per embryos to compare the difference among groups. Statistical analysis was performed using Student's unpaired t-test. Differences were considered significant for $p < 0.05$.

MYO1F mutation screening in FNMTC pedigrees

PCR primers for human *MYO1F* (NM_012335) were designed with Primer3 v4.0 (http://primer3.ut.ee) and are available on request. Genomic DNA extracted from peripheral blood was amplified according to standard PCR conditions and PCR products were analyzed by direct sequencing, as reported in the Supporting Data file.

P1 pAltermax MYO1F exon 7-minigene generation

PCR of *MYO1F* genomic region encompassing exons 7 and 8 was performed using primer forward 5' GGGGAATTCAGAAGGGAAGAGAGGCAAGG-3', inserting an *EcoRI* restriction site, and primer reverse 5'-CCCTCTAGAAACTCAGGAGGGTTTCTGGG-3', inserting an *XbaI* restriction site from a heterozygous carrier. We generated the mini-gene reporter as previously described [5]. The PCR products were cloned into the digested P1 pAltermax and plasmids sequenced in order to identify the plasmids with the wt or the variant alleles and the splicing alteration analysis was described as reported in [5] and in the Supporting Data.

Structural modelling

Modelling of the protein structure was performed adopting a building obtained by comparison procedures based on MODELLER (https://salilab.org/modeller/). The template was MYO1C_HUMAN (PDB code: 4BYF_A), and the final structural superimposition indicated a 45% sequence identity among the computed and experimental structures. Given the coverage of the template to the target, modelling

was possible in the protein region spanning amino acids 16-714. From structural superimposition, it was also possible to locate the ATP-binding domain.

Statistical analysis

Statistical analyses were performed using the one-way analysis of variance (ANOVA) with Tukey's Multiple Comparison test. All tests were completed using Prism (GraphPad, San Diego, CA, USA). A $p < 0.05$ was considered statistically significant. All experiments were carried out at least in triplicates.

Results

Identification of a novel missense mutation in MYO1F conferring tumor-like properties to thyroid cells

WES was performed in three members of the original TCO family where the linkage locus was identified [8] (II-3, II-4, III-7; Figure 1A), in two individuals affected by thyroid carcinoma and one affected by thyroid adenoma, all with oncocytic features. All variants were queried with ANNOVAR and filtered based on dbSNP database annotation. Potentially deleterious mutations were selected according to their functional class, and prioritization was given to those lying in the chr19p13.2 linkage region and present in all three cases. A unique novel heterozygous variant in the linkage interval shared by all 3 individuals fulfilled the criteria for pathogenicity: the mutation c.400G>A in *MYO1F* cDNA (NM_012335), leading to a missense p.134G>S substitution, predicted to be damaging by PolyPhen-2 and Provean (Table S2), not present in the NHLBI Exome Sequencing Project (ESP) or in Exome Aggregation (ExAc) databases, and absent from 1000 in-house control chromosomes. The variant co-segregated with the carcinoma/adenoma phenotype in the family and appeared to be a likely candidate for the NMTC gene residing at 19p13.2 (Figure 1A).

MYO1F consists of 28 exons encoding a 1098-amino-acid protein of the class of unconventional myosins [14]. The p.134G>S amino acid change resides in a very well conserved position in the ATP-binding domain of the protein. Since thyroid tumor tissue from patients was not available for additional studies, we generated cell models stably expressing the wild-type (wt) or mutant MYO1F (mut) after transfection with the corresponding episomal plasmids, and a control cell line stably expressing the corresponding empty vector, pCMV6, via G418 selection. We used highly differentiated and functional FRTL-5 rat thyroid cell line [9] in order to reveal dominant-negative effects of the MYO1F variant. The p.134G>S mutation was inserted by site-directed mutagenesis in the construct encoding wt *MYO1F* in frame with the DDK tag. Western blotting with anti-DDK antibody in stably transfected cells showed that both wt and mut proteins were expressed in similar amounts (Figure 1B). Stable cell lines expressing either the wt or the mut MYO1F protein were tested for their tumorigenic potential in comparison with cells transfected with the empty vector. A significant increase in the number of colonies in anchorage-dependent and independent growth was observed in mut cells, compared to cells expressing either the empty vector or the wt recombinant protein (one-way ANOVA $p < 0.0001$, Figures 1C and 1D). Anchorage-independent growth was monitored as colony formation in soft agar. Mutant MYO1F-expressing cells showed a significant increase in colony formation in soft agar, compared to cells stably transfected with the wt protein or the empty vector (ordinary one-way ANOVA $p=0.0005$; Figure 1D, lower panel).

The wound-healing assay showed that mutant cells had a significantly greater invasive potential after 7 days in culture, compared to cells stably transfected with the

empty vector or the wt protein, as quantified with *TScratch* software [10], (ordinary one-way ANOVA p=0.0024; Figure 1E).

In order to relate the observed changes in growth to the activation of specific cellular pathways, we investigated different kinases with key roles in cell proliferation and migration, including Akt and ERK1/2. We found a specific increase in the phosphorylation of ERK1/2 kinases in cells expressing the mutant protein, in particular for the p42 isoforms (Figures 1F, G; p=0.0042, empty *vs* pCMV6 MYO1F G134S). Taken together, these findings support a role for the MYO1F mutation in the modulation of tumorigenic potential in vitro (i.e. in the modulation of proliferation and invasivity).

Mutant MYO1F p.134G>S stimulates proliferation in zebrafish embryos

In order to analyze the pro-proliferative function of MYO1F *in-vivo*, we evaluated the effects of the human p.134G>S MYO1F protein in zebrafish (*Danio rerio*) embryos. The zebrafish genome encodes a single *myo1f* orthologue (GenBank ref seq. NM_001256671.2; NP_001243600.1), with 85% similarity and 76% identity at amino acidic level to human MYO1F. Notably, the position corresponding to human Glycine 134 is conserved in the zebrafish Myo1f protein, indicating a putative functional role of this aminoacidic residue (Figure S2).

To test whether the mutant MYO1F variant can induce cell proliferation *in vivo,* one-cell stage embryos were injected with either wild type or p.134G>S MYO1F mutated mRNA. At 48 hours post fertilizations (hpf) the injected embryos were fixed and stained with antibodies against phospho-histone H3 (pH3), a widely used marker to reveal cell mitosis in zebrafish [15-17]. Embryos injected with the mutant mRNA showed a significant increase in the number of pH3-positive cells, compared to their siblings injected with the MYO1F wild-type allele (Figures 2A, B). In particular we

observed an increased number of mitotic cells, especially in the caudal region (p-value < 0.0001, Figure 2C) indicating that, when ubiquitously expressed, the MYO1F mutant protein can induce proliferation also in zebrafish embryos.

Iodide influx is not altered by the mutation MYO1F p.134G>S

FRTL-5 cells are highly differentiated thyroid cells and a suitable model to measure iodide transport *in vitro*. We measured iodide uptake by live cell imaging after transient transfection with a vector encoding YFP-H148Q/I152L, a modified yellow Fluorescent Protein (YFP) whose fluorescence is quenched by I^- in a concentration-dependent manner [11, 12]. We did not detect any differences in I^- uptake between the different cell lines (one-way ANOVA p=0.4816; Figures S1A, B).

The mutation MYO1F p.134G>S alters the mitochondrial network

Since the oncocytic phenotype is characterized by mitochondrial hyperplasia in the tumors of affected individuals of the TCO family [8], we analyzed the mitochondrial network of stably-transfected FRTL-5 cells by live-cell microscopy using the MitoTracker Green probe. Mitochondria in the mutant cell lines appeared more fragmented compared to mitochondria in wt and empty cell lines (Figure 3A), as shown by the significant increase in circularity value of mutant cells mitochondria when compared to wt and empty cell mitochondria (Figure 3B). The total mitochondrial mass was significantly greater in mutant cell lines, as determined by MitoTracker fluorescence quantification, normalized for cell viability using a resazurin-based assay (ordinary one-way ANOVA p<0.0001; Figure 3C). Since an impaired mitochondrial network may alter mitochondrial function, we measured the mitochondrial membrane potential and oxidative phosphorylation (OXPHOS) activity of the different cell lines. The mitochondrial membrane potential was measured with the probe JC-1 [18, 19], and normalized for cell viability using a resazurin-based

assay. No differences were found between empty vector-expressing cells, wt and mutant cells (one-way ANOVA p=0.0720; Figure 3D). Concurrently, there were no differences in respiratory activity between the different cell lines under basal conditions (one-way ANOVA p=0.5014, Figure 3E) and in the ratio of FCCP/oligomycin-treated cells (one-way ANOVA p=0.3900; Figure 3F). Extracellular lactate measurement also showed no changes between the different cell lines (ordinary one-way ANOVA p=0.4069; Figure S3A).

Reactive Oxygen Species (ROS) are elevated in FRTL-5 cells expressing MYO1F p.134G>S

Since differentiated thyroid cells produce a great amount of H_2O_2 necessary for thyroid hormone synthesis [20], we investigated whether ROS production in transfected FRTL-5 cell lines was deranged by the MYO1F mutation.

Intracellular ROS levels, measured with the fluorescent probe DCF-DA, were significantly increased in the mutant cells (one-way ANOVA p= 0.0015, Figure 4A). To understand whether this phenomenon was due to alterations/decreases of intracellular ROS detoxifying enzymes, we performed western blotting analysis of catalase, SOD2 (mitochondrial Manganese Superoxide Dismutase) and Peredoxin-3 (Prx3), using GAPDH as endogenous reference. The steady state levels of the analyzed proteins were not significantly different between all cell lines (Figure 4B and Figures S4A-C; one-way ANOVA p=0.1328 for catalase, p=0.8592 for SOD2, p=0.6837 for Prx3).

In order to measure extracellular ROS, we used the fluorescent probe Amplex Red, which is unable to cross the plasma-membrane. In this case we observed a significantly higher amount of extracellular ROS in mutant cell lines, compared to the empty vector-transfected cells and the wt ones. Moreover, we detected, a significant

decrease in extracellular ROS in the cells expressing MYO1F wt, when compared to the empty vector (one-way ANOVA p=0.0004; pCMV6-empty vs pCMV6-MYO1F wt p<0.05; pCMV6-MYO1F wt vs pCMV6-MYO1F G134S p<0.001; Figure 4C).

Mutation screening of human MYO1F in FNMTC patients

In order to identify additional patients carrying predisposing germline mutations in *MYO1F*, we performed a mutation screening via Sanger sequencing of genomic DNA from peripheral blood of 192 independent FNMTC cases. These patients represented a heterogeneous group of cases affected by PTC/FTC, but oncocytic features were not always investigated and these data were available only for a small subgroup of patients (Table S1). Nevertheless, we identified several rare/novel coding variants in *MYO1F* (Table 1), including a rare silent change in exon 7, that was present in both the affected individuals of the corresponding family, from whom DNA was available (Figure S5A). This change potentially removed an exonic sequence enhancer (ESE) in exon 7, as predicted by the ESE Finder v3.0 program (Figure S5B). The change, corresponding to the genomic coordinates chr19:g.8616995C>T (rs184748543), has a M.A.F. (Minor Allele Frequency) of 0.003064 in the whole Exome Aggregation database (ExAC), and a M.A.F. of 0.004166 in individuals of European ancestry.

rs184748543 alters the inclusion of exon 7 in MYO1F transcript

In order to study whether the exon 7 variant hampers the inclusion of this exon in the final *MYO1F* transcript, we generated a minigene plasmid carrying either the wt or mutant sequence, and transfected simian COS7 cells in order to study transcription (Figures 5A, B). RT-PCR with minigene-specific synthetic primers and direct sequencing revealed that the wt exon was correctly spliced, whereas the mutant transcript lacked exon 7 (Figure 5C). This altered transcript is predicted to produce a shorter MYO1F protein, with an in-frame deletion of 43 amino acids (G169-Q212) in

the motor domain of MYO1F, that may alter the structure of the ATP-binding domain in the molecular motor of MYO1F (residues 110-117 and 162-166; Figure 5D).

Discussion

The etiology of differentiated thyroid cancer is still poorly understood, but this type of cancer is influenced by both genetic and environmental factors. Large genome-wide case-control association studies have identified genetic variants conferring NMTC susceptibility in the general population [21-23]. A number of common SNPs have been reported to be associated with NMTC risk, but few studies have been conducted in high-risk NMTC families to examine the transmission of the risk allele to the affected members.

In the present study, we report the identification of MYO1F as the gene mutated at the TCO locus. We provide functional evidence that the MYO1F p.134 G>S mutation leads to an increased oncogenic potential *in vitro*, in terms of cell growth and invasion. FRTL-5 cells, a cell model resembling a functional thyrocyte [9], stably transfected with the plasmid encoding mutant MYO1F p.134G>S generated significantly more colonies in soft agar and showed a significantly greater invasive potential compared to cells stably transfected with the empty vector or with wt *MYO1F*.

These *in vitro* data were supported by *in vivo* findings in zebrafish, showing that the mutant MYO1F p.134G>S, when overexpressed, can induce proliferation in whole vertebrate embryos, supporting the idea that the novel missense change identified in exon 5 of *MYO1F* is the causative mutation at the TCO locus.

The TCO locus in the original pedigree was associated with an oncocytic phenotype, i.e. enriched in mitochondria [8]. Previous work by our group uncovered a tight correlation between the co-occurrence of mitochondrial DNA (mtDNA) alterations in

oncocytic thyroid cancer, and a marked dysfunction of OXPHOS complexes, in particular complex I [24-26]. Since thyroid follicular cells generate H_2O_2 by membrane-bound dual oxidases for the synthesis of thyroid hormones, these cells are at increased risk of oxidative stress and ROS-mediated DNA damage. Indeed, an imbalance between pro- and anti-oxidative factors has been suggested as an important mechanism in thyroid tumorigenesis [20,27]. Oxidative stress generated by mitochondrial dysfunction can also promote migration and stimulate MAPK-mediated cell death. We therefore sought to evaluate: i) the functionality of the mitochondrial respiratory chain as a whole; ii) the response to oxidative stress of FRTL-5 cells stably expressing the wt or mutant recombinant MYO1F protein, compared to cells expressing the empty-vector. We found that the mitochondrial membrane potential and OXPHOS activities were similar in all cell lines, suggesting that mitochondria were still functional. However, analysis of the mitochondrial network by live-cell visualization revealed that in the mutant cell lines, mitochondria appeared as separated rod-shaped organelles. The mitochondrial features of mutant MYO1F cells were therefore reminiscent of the oncocytic features described previously in the tumor tissues of the patients carrying the p.134G>S change [8].

In our experimental setting, we found that cells with the MYO1F p.134 G>S mutation, in addition to having an altered mitochondrial network, produced significantly more intracellular and extracellular ROS. It has been reported that the establishment and maintenance of a transformed state is related to the presence of extracellular ROS, in particular superoxide anion generated by a specific membrane-associated NADPH-oxidase, NOX1 [28]. In fact, oncogenic activation of proliferative/mitogenic pathways has been associated with increased ROS production due to activation of the membrane-bound NADPH oxidases [29]. Extensive analysis

of tumor cell lines derived from different tissues, including thyroid carcinomas, has shown that they were all characterized by extracellular ROS generation, not found in cells derived from normal tissues [30]. This is paralleled by our findings, since extracellular ROS production was increased only in FRTL-5 cells expressing the mutant MYO1F p.134G>S protein, suggesting that the mutation is sufficient to generate a transformed phenotype.

Since the "mitochondria-rich" phenotype may be under-reported by histologic analysis [25], we screened additional FNMTC patients in order to identify other *MYO1F* germline variants that could predispose to thyroid tumor development. However, the available samples represented a heterogeneous group of familial cases affected by NMTC, and the high genetic heterogeneity of thyroid cancer could have hampered the discovery of a number of additional predisposing variants. Indeed, only a rare variant identified in two affected sibs in exon 7 may have a damaging role, since it promotes the skipping of the exon from mature mRNA. Although the allele frequency of this variant was not significantly different from the one present in ExAc public database, it may act as a predisposing risk allele with variable penetrance, as recently shown for in-frame *USF3* variants in differentiated thyroid cancer [31].

Since no RNA from fresh or formalin-embedded tissues from these patients were available, to evaluate the *in vivo* expression of the transcript we performed *in vitro* analysis using a splicing minigene [5], confirming the exon 7 skipping. The altered transcript generated an in-frame deletion of 43 amino acids in the ATP-binding domain of MYO1F, while retaining the F (filamentous) actin-binding module. F-actin is one of the few known interactors of MYO1F [14] and has been recently implicated in mitochondrial fission control [32]. Blockade of F-actin polymerization / depolymerization altered the mitochondrial network [33]. Structural modeling

predicts that MYO1F exon 7 skipping would modify the structure of the ATP binding site. Similarly to what has been observed in other autosomal dominant disorders due to mutations in myosin genes, such as MYH9 [34,35], the modified conformation of MYO1F may block actin filament recycling, therefore concurrently altering the mitochondrial network organization, as observed for the G134S mutation.

Our study shows that defective MYO1F promotes the development of an oncocytic phenotype, i.e. mitochondrial proliferation, indicating that this cellular characteristic can develop not only from mitochondrial DNA defects [24-26], but also from nuclear defects in specific genes, i.e. *MYO1F*. Mitochondrial dysfunction and stress has been widely related to cancer, in particular in thyroid cancer predisposition [36, 37]. More broadly, an altered mitochondrial function is a hallmark of many cancers, although the nature of functional modification depends on the type of cancer [38]. Recent data have shown the contribution of mitochondrial dynamics towards tumor initiation and progression, although the exact mechanism is not known. Excessive fission and reduced fusion is a feature of many tumors [39-41]. For example, in human pancreatic cancer, expression of oncogenic Ras / activation of MAPK pathway induces ERK2-mediated Drp1 phosphorylation leading to increased mitochondrial fragmentation [42]. Moreover, inhibition of this phosphorylation in xenografts is sufficient to block tumor growth [42]. It is becoming increasingly clear that mitochondrial fission and fusion play a critical role in quality control and mitochondrial damage/repair in cancer. Therefore, our data showing a fragmented mitochondrial network due to MYO1F p.134G>S mutation highlight a potential novel pathway that may be deranged in thyroid cancer, i.e. an altered myosin/F-actin regulated interaction [14].

To date, no other mutations have been reported in myosin-encoding genes in thyroid cancer, however it is interesting that MYH9, a non-muscle myosin involved in sensorineural deafness and thrombocytopenia [35], has recently been found to regulate the ncRNA genes *PTCSC2* and *FOXE1* at the 9q22 thyroid cancer susceptibility locus [43]. In the TCGA database, somatic mutations in *MYO1F* are reported in 352 cases from various cancer types (Supplementary Figure S6A). The mutation identified at the TCO locus p.134G>S was not reported. In the COSMIC database several mutations are present in MYO1F in different types of cancer (Supplementary Figure S6B), but only a somatic variant is reported in thyroid carcinoma (COSM4132813). However, *MYO1F* overexpression was reported in 24/513 (4.68%) cases (Supplementary Figure S6C). These and our data suggest that MYO1F dysregulation may predispose to cancer in a subgroup of cases. Indeed, the oncocytic phenotype, observed in the family with the p.134G>S mutation, represents a specific, though rare, group of thyroid neoplasms, in which *MYO1F* mutation screening may be more relevant than in other NMTC cancer cases. The identification of the molecular cause(s) of specific thyroid cancer subtypes will help tailor patients' treatment for a more personalized therapy.

Acknowledgements

We thank all patients and families that participated in the study. We would like to thank Mr. F. Baccianti, Dr. F. Bianco and Dr. G. Zuccheri for technical support in cell imaging and Dr. I. Kurelac for helpful suggestions and discussion. We would like to thanks Dr. L. Pivotti and Dr. M. Milanetto for their help in managing Padua Zebrafish Facility.

URL

Catalogue of Somatic Mutations in Cancer (COSMIC): http://cancer.sanger.ac.uk/

ESEfinder 3.0: rulai.cshl.edu/tools/ESE/

ESP: evs.gs.washington.edu/EVS/

Exome Aggregation Consortium (ExAc): http://exac.broadinstitute.org/

MODELLER: https://salilab.org/modeller/

PolyPhen-2: genetics.bwh.harvard.edu/pph2PROVEAN (including SIFT): provean.jcvi.org/

Primer 3: primer3.ut.ee

The Cancer Genome Atlas (TCGA): https://tcga-data.nci.nih.gov/

References

1. Malchoff CD and Malchoff DM. Familial nonmedullary thyroid carcinoma. *Cancer Control* 2006; 13: 106–10.

2. Eng, C. PTEN: One gene, many syndromes. *Hum. Mutat.* 2003 22, 183–198.

3. Ni Y, Zbuk KM, Sadler T, Patocs A, Lobo G, Edelman E, Platzer P, Orloff MS, Waite KA, Eng C. Germline mutations and variants in the succinate dehydrogenase genes in Cowden and Cowden-like syndromes. *Am J Hum Genet.* 2008 83(2):261-268.

4. Bonora E, Tallini G and Romeo G. Genetic Predisposition to Familial Nonmedullary Thyroid Cancer: An Update of Molecular Findings and State-of-the-Art Studies. *J Oncol* 2010; 2010: 385206.

5. Bonora E, Evangelisti C, Bonichon F, Tallini G and Romeo G. Novel germline variants identified in the inner mitochondrial membrane transporter TIMM44 and

their role in predisposition to oncocytic thyroid carcinomas. *Br J Cancer* 2006; 95: 1529–36

6. Bonora E, Rizzato C, Diquigiovanni C, Oudot-Mellakh T, Campa D, Vargiolu M, Guedj M, NMTC Consortium, McKay JD, Romeo G, Canzian F and Lesueur F. The FOXE1 locus is a major genetic determinant for familial nonmedullary thyroid carcinoma. *Int J Cancer* 2014; 134: 2098–107.

7. Rio Frio T, Bahubeshi A, Kanellopoulou C, Hamel N, Niedziela M, Sabbaghian N, Pouchet C, Gilbert L, O'Brien PK, Serfas K, Broderick P, Houlston RS, Lesueur F, Bonora E, Muljo S, Schimke RN, Bouron-Dal Soglio D, Arseneau J, Schultz KA, Priest JR, Nguyen VH, Harach HR, Livingston DM, Foulkes WD and Tischkowitz M. DICER1 mutations in familial multinodular goiter with and without ovarian Sertoli-Leydig cell tumors. *JAMA* 2011; 305: 68–77.

8. Canzian F, Amati P, Harach HR, Kraimps JL, Lesueur F, Barbier J, Levillain P, Romeo G and Bonneau D. A gene predisposing to familial thyroid tumors with cell oxyphilia maps to chromosome 19p13.2. *Am J Hum Genet* 1998; 63: 1743–8.

9. Meli A, Perrella G, Curcio F and Ambesi-Impiombato FS. In vitro cultured cells as probes for space radiation effects on biological systems. Mutat Res 1999; 430: 229–34.

10. Gebäck T, Schulz MM, Koumoutsakos, Detmar M. TScratch: a novel and simple software tool for automated analysis of monolayer wound healing assays. Biotechniques 2009; 46: 265–74.

11. Rhoden KJ, Cianchetta S, Stivani V, Portulano C, Galietta LJ and Romeo G. Cell-based imaging of sodium iodide symporter activity with the yellow fluorescent protein variant YFP-H148Q/I152L. Am J Physiol Cell Physiol 2007; 292: C814–23.

12. Rhoden KJ, Cianchetta S, Duchi S and Romeo G. Fluorescence quantitation of thyrocyte iodide accumulation with the yellow fluorescent protein variant YFP-H148Q/ I152L. Anal Biochem 2008; 373: 239–46.

13. Chazotte B. Labeling mitochondria with MitoTracker dyes. Cold Spring Harb Protoc 2011; 2011: 990–92.

14. Kim SV, Mehal WZ, Dong X, Heinrich V, Pypaert M, Mellman I, Dembo M, Mooseker MS, Wu D and Flavell RA. Modulation of cell adhesion and motility in the immune system by Myo1f. Science 2006; 314: 136–39.

15. Verduzco D and Amatruda JF. Analysis of cell proliferation, senescence, and cell death in zebrafish embryos. Methods Cell Biol. 2011; 101: 19-38.

16. Mendieta-Serrano MA, Schnabel D, Lomelí H and Salas-Vidal E. Cell proliferation patterns in early zebrafish development. *Anat Rec (Hoboken)*. 2013; 296: 759-73.

17. Luo N, Li H, Xiang B, Qiao L, He J, Ji Y, Liu Y, Li S, Lu R, Li Y, Meng W, Wu Y, Xu H and Mo X. Syndecan-4 modulates the proliferation of neural cells and the formation of CaP axons during zebrafish embryonic neurogenesis. *Sci Rep*. 2016; 6: 25300.

18. Smiley ST, Reers M, Mottola-Hartshorn C, Lin M, Chen A, Smith TW, Steele GD Jr and Chen LB. Intracellular heterogeneity in mitochondrial membrane potentials revealed by a J-aggregate-forming lipophilic cation JC-1. *Proc Natl Acad Sci USA* 1991; 88: 3671–75.

19. Chazotte B. Labeling mitochondria with JC-1. *Cold Spring Harb Protoc* 2011; 2011: 9.

20. Yoshihara A, Hara T, Kawashima A, Akama T, Tanigawa K, Wu H, Sue M, Ishido Y, Hiroi N, Ishii N, Yoshino G and Suzuki K. Regulation of dual oxidase expression and H2O2 production by thyroglobulin. Thyroid 2012; 22: 1054–62.

21. Cavaco BM, Batista PF, Sobrinho LG and Leite V. Mapping a new familial thyroid epithelial neoplasia susceptibility locus to chromosome 8p23.1-p22 by high- density single-nucleotide polymorphism genome-wide linkage analysis. *J Clin Endocrinol Metab* 2008; 93: 4426–30.

22. Jazdzewski K, Murray EL, Franssila K, Jarzab B, Schoenberg DR and de la Chapelle A. Common SNP in pre-miR-146a decreases mature miR expression and predisposes to papillary thyroid carcinoma. *Proc Natl Acad Sci USA* 2008; 105: 7269–74.

23. Gudmundsson J, Sulem P, Gudbjartsson DF, Jonasson JG, Sigurdsson A, Bergthorsson JT, He H, Blondal T, Geller F, Jakobsdottir M, Magnusdottir DN, Matthiasdottir S, Stacey SN, Skarphedinsson OB, Helgadottir H, Li W, Nagy R, Aguillo E, Faure E, Prats E, Saez B, Martinez M, Eyjolfsson GI, Bjornsdottir US, Holm H, Kristjansson K, Frigge ML, Kristvinsson H, Gulcher JR, Jonsson T, Rafnar T, Hjartarsson H, Mayordomo JI, de la Chapelle A, Hrafnkelsson J, Thorsteinsdottir U, Kong A and Stefansson K. Common variants on 9q22.33 and 14q13.3 predispose to thyroid cancer in European populations. *Nat Genet* 2009; 41: 460–64.

24. Bonora E, Porcelli AM, Gasparre G, Biondi A, Ghelli A, Carelli V, Baracca A, Tallini G, Martinuzzi A, Lenaz G, Rugolo M and Romeo G. Defective oxidative phosphorylation in thyroid oncocytic carcinoma is associated with pathogenic mitochondrial DNA mutations affecting complexes I and III. *Cancer Res* 2006; 66: 6087–96.

25. Gasparre G, Porcelli AM, Bonora E, Pennisi LF, Toller M, Iommarini L, Ghelli A, Moretti M, Betts CM, Martinelli GN, Ceroni AR, Curcio F, Carelli V, Rugolo M, Tallini G and Romeo G. Disruptive mitochondrial DNA mutations in complex I subunits are markers of oncocytic phenotype in thyroid tumors. *Proc Natl Acad Sci USA* 2007; 104: 9001–6.

26. Porcelli AM, Ghelli A, Ceccarelli C, Lang M, Cenacchi G, Capristo M, Pennisi LF, Morra I, Ciccarelli E, Melcarne A, Bartoletti-Stella A, Salfi N, Tallini G, Martinuzzi A, Carelli V, Attimonelli M, Rugolo M, Romeo G and Gasparre G. The genetic and metabolic signature of oncocytic transformation implicates HIF1alpha destabilization. *Hum Mol Genet* 2010; 19: 1019–32.

27. Bauer G. Targeting extracellular ROS signaling of tumor cells. *Anticancer Res* 2014; 34: 1467–82

28. Laurent E, McCoy JW, Macina RA, Liu W, Cheng G, Robine S, Papkoff J and Lambeth JD. Nox1 is over-expressed in human colon cancers and correlates with activating mutations in K-Ras. *Int J Cancer* 2008; 123: 100–7.

29. Carvalho DP and Dupuy C. Role of the NADPH Oxidases DUOX and NOX4 in Thyroid Oxidative Stress. *Eur Thyroid J* 2013; 2: 160–7.

30. Irani K, Xia Y, Zweier JL, Sollott SJ, Der CJ, Fearon ER, Sundaresan M, Finkel T and Goldschmidt-Clermont PJ. Mitogenic signaling mediated by oxidants in Ras- transformed fibroblasts. *Science* 1997; 275: 1649–52.

31. Ni Y, Seballos S, Fletcher B, Romigh T, Yehia L, Mester J, Senter L, Niazi F, Saji M, Ringel MD, LaFramboise T, Eng C. Germline compound heterozygous poly- glutamine deletion in USF3 may be involved in predisposition to heritable and sporadic epithelial thyroid carcinoma. Hum Mol Genet. 2017; 26(2):243-257.

mitochondrial fission. *Curr Biol 2013*; 23: R891–9.
32. Bui HT and Shaw JM. Dynamin assembly strategies and adaptor proteins in
33. Li S, Xu S, Roelofs BA, Boyman L, Lederer WJ, Sesaki H and Karbowski M. Transient assembly of F-actin on the outer mitochondrial membrane contributes to mitochondrial fission. *J Cell Biol* 2015; 208: 109–23.

34. Seri M, Cusano R, Gangarossa S, Caridi G, Bordo D, Lo Nigro C, Ghiggeri GM, Ravazzolo R, Savino M, Del Vecchio M, d'Apolito M, Iolascon A, Zelante LL, Savoia A, Balduini CL, Noris P, Magrini U, Belletti S, Heath KE, Babcock M, Glucksman MJ, Aliprandis E, Bizzaro N, Desnick RJ, Martignetti JA. Mutations in MYH9 result in the May-Hegglin anomaly, and Fechtner and Sebastian syndromes. The May-Heggllin/ Fechtner Syndrome Consortium. *Nat Genet.* 2000 26(1):103-105. 35. Seri M, Pecci A, Di Bari F, Cusano R, Savino M, Panza E, Nigro A, Noris P, Gangarossa S, Rocca B, Gresele P, Bizzaro N, Malatesta P, Koivisto PA, Longo I, Musso R, Pecoraro C, Iolascon A, Magrini U, Rodriguez Soriano J, Renieri A, Ghiggeri GM, Ravazzolo R, Balduini CL, Savoia A. MYH9-related disease: May-Hegglin anomaly, Sebastian syndrome, Fechtner syndrome, and Epstein syndrome are not distinct entities but represent a variable expression of a single illness. *Medicine (Baltimore)*. 2003,82:203-215.

36. Yu W, Ni Y, Saji M, Ringel MD, Jaini R, Eng C. Cowden syndrome-associated germline succinate dehydrogenase complex subunit D (SDHD) variants cause PTEN-mediated down-regulation of autophagy in thyroid cancer cells. *Hum Mol Genet*. 2017;26(7):1365-1375.

37. De Luise M, Girolimetti G, Okere B, Porcelli AM, Kurelac I, Gasparre G. Molecular and metabolic features of oncocytomas: Seeking the blueprints of indolent cancers. *Biochim Biophys Acta*. 2017;1858(8):591-601

38. Srinivasan S, Guha M, Kashina A, Avadhani NG. Mitochondrial dysfunction and mitochondrial dynamics-The cancer connection. *Biochim Biophys Acta.* 2017;1858(8):602-614.

39. Inoue-Yamauchi A, Oda H. Depletion of mitochondrial fission factor DRP1 causes increased apoptosis in human colon cancer cells, *Biochem. Biophys. Res. Commun.* 2012; 421: 81–85.

40. Zhao J, Zhang J, Yu M, Xie Y, Huang Y, Wolff DW, Abel PW, Tu Y. Mitochondrial dynamics regulates migration and invasion of breast cancer cells. *Oncogene* 32, 40: 4814–4824.

41. Ferreira-da-Silva A, Valacca C, Rios E, Pópulo H, Soares P, Sobrinho-Simões M, Scorrano L, Máximo V, Campello S. Mitochondrial dynamics protein Drp1 is overexpressed in oncocytic thyroid tumors and regulates cancer cell migration, PLoS One 2015; 10: e0122308.

42. Kashatus JA, Nascimento A, Myers LJ, Sher A, Byrne FL, Hoehn KL, Counter CM, Kashatus DF. Erk2 phosphorylation of Drp1 promotes mitochondrial fission and MAPK driven tumor growth. *Mol. Cell*. 2015; 57: 537–551.

43. Wang Y, He H, Li W, Phay J, Shen R, Yu L, Hancioglu B and de la Chapelle A. MYH9 binds to lncRNA gene PTCSC2 and regulates FOXE1 in the 9q22 thyroid cancer risk locus. *Proc Natl Acad Sci U S A*. 2017; 114: 474-479.

Table 1: Rare coding variants identified in *MYO1F*-targeted mutation screening

Chr19 genomic position (hg19)	Amino acid change (NP_036467)	M.A.F in famNMTC (N=192)	M.A.F. in ExAc
g.8616995 C>T rs184748543	p.186K=[a]	0.0026[b]	0.003064
g.8615552C>T rs201962739	p.266P=	0.0026	0.0012
g.8615513C>G	p.368G=[a]	0.0026[c]	0
g.8610599G>T	p.430I=	0.0026	0
g.8587411C>T rs201982814	p.1024V>M	0.0026[d]	0.007326

a) SNV not changing the corresponding amino acid, but with an altered ESE (Exonic Sequence Enhancer) profile compared to wild-type cDNA, and removing SR-binding domains.
b) SNV co-segregating with the NMTC phenotype in the available members of the corresponding family.
c) SNV not segregating with the NMTC phenotype in the corresponding families.
d) Missense variant predicted to be "benign" (PolyPhen-2) and "tolerated" (SIFT).

Figure Legends

Figure 1. Study of MYO1F p.134G>S variant. (A) Pedigree of the TCO family: electropherograms of the sequences of available family members, showing the co-segregation of the change (in red) with the oncocytic carcinoma (black)/adenoma (grey) phenotype. (B-F) Functional analysis of the MYO1F p.134G>S variant. All experiments were repeated at least three times. (B) Western blot analysis showing the recombinant MYO1F protein in stably expressing FRTL-5 cells, using a specific anti-DDK antibody. (C) SRB assay showed a significant increase in the number of colonies formed by FRTL-5 expressing the mutant MYO1F protein, compared to cells

expressing either the empty vector or the wt protein (D) Growth in soft agar: FRTL-5 cells expressing the MYO1F mutant protein p.134G>S significantly generated more colonies, compared to the empty and the cells expressing the wt protein. (E) Wound healing assay: FRTL-5 cells expressing the MYO1F mutant protein p.134G>S filled the gap significantly faster compare to the other two cell lines. (F, G) Western blotting analysis of ERK1/2 phosphorylation in the three cell lines and densitometric quantification.

Figure 2. Proliferation analysis in zebrafish overexpressing either wild-type or mutant MYO1F p.134G>S: (A-B) Immunostaining of Phospho-histone H3 (pH3) performed in 48 hpf zebrafish larvae. An increase of cell proliferation can be observed in embryos injected with mutant MYO1F mRNA compared with embryos injected with the wild-type transcript of MYO1F. C) Quantification of pH3 -positive cells in injected embryos (48 hpf) was performed counting the number of mitotic cells along the trunk of each fish. For each group, 22 embryos were analyzed (MYO1F_MUT: 25.45 ± 2.584; MYO1F_WT: 8.727 ± 1.445). ***P < 0.001, Student's unpaired t-test.

Figure 3. Mitochondrial defects in FRTL-5- MYO1F p.134G>S cells.

(A) Representative fluorescence images of pCMV6-empty, pCMV6-MYOF wild type and pCMV6-MYOF G134-S treated with Mitotracker Green to evaluate mitochondrial network. The cells expressing the mutant protein show more circular (B) and more abundant (C) mitochondria and more fragmented mitochondrial network in comparison with wild type and cells bearing empty vector. MitoTracker signal quantification was normalized on viable cell number assessed by resazurin-based assay. (D) To evaluate the mitochondrial membrane potential cells were treated with JC-1 fluorescent probe. In (D) the quantification of aggregate/monomer signal of JC-1

normalized on viable cell number is shown. Cell viability was assessed by resazurin-based method. (E) Basal rate of oxygen consumption in pCMV6-empty, pCMV6-MYOF wild type and pCMV6-MYOF G134>S cells. (F) shows the ratio between oxygen consumption in the presence of oligomycin and in the presence of FCCP (uncoupled respiration).

Figure 4. ROS production. (A) Intracellular ROS production measured by DCFDA fluorescent probe. Data show a significant ROS production increase in the FRTL-5 cells expressing MYO1F p.134G>S in comparison to wild type and cells bearing the empty pCMV6 vector. Data are expressed as arbitrary fluorescence units ± standard deviation, normalized on viable cell number. (B) Representative western blot analysis showing the expression of detoxifying enzymes (catalase, SOD2 and Prx3) in the three cell lines. GAPDH was used as endogenous loading control. (C) Extracellular ROS production measured by Amplex red fluorescent probe. Data show that FRTL-5 cells expressing MYO1F p.134G>S presented the highest levels of extracellular ROS, whereas the cells expressing the wt protein presented a reduced amount of extracellular ROS. Data are expressed as arbitrary fluorescence units ± standard deviation normalized on viable cell number. Cell viability was assessed by resazurin-based method.

Figure 5. MYO1F rs184748543. (A) Map of the minigene plasmid, showing the genomic insert of the wt and mutant alleles (red arrows). (Blue arrows= position of the primers used for the specific RT-PCR). (B) RT-PCR of COS7-transfected with the *MYO1F* allele-specific mini-genes. *Upper panel*: predicted final transcripts generated by the correct splicing of mini-gene-specific exons (blue) and *MYO1F*-specific exons (grey). *Lower panel*: 2% agarose gel image (left) of the RT-PCR products, showing the different sizes of the transcripts and corresponding electropherograms (right): the

wild-type *MYO1F* allele promoted the inclusion of the exon 7 in the final transcript, whereas the mutant allele induced an exon skipping in the final transcript, as predicted by the removal of the ESE in the exon 7. (D) Structure prediction of the MYO1F molecular motor region, with the ATP-binding region highlighted in green. In pink the residues corresponding to exon 7, in red the ion of magnesium.

Figure 1

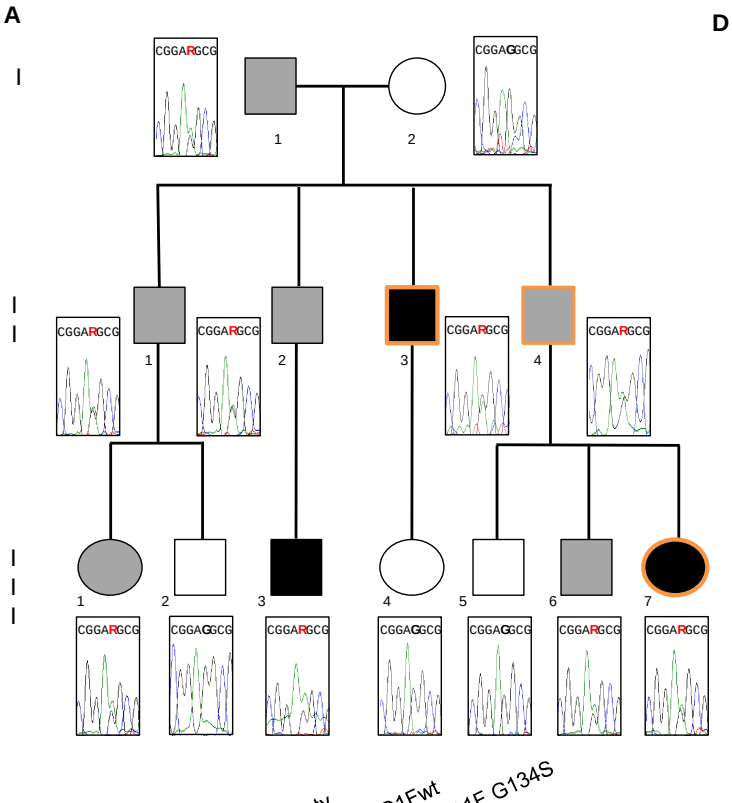
A
I
II
III
CGGARGCG
CGGAGGCG
1
2
3
4
5
6
7

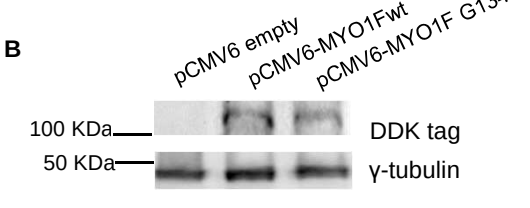
B
pCMV6 empty
pCMV6-MYO1Fwt
pCMV6-MYO1F G134S
100 KDa
50 KDa
DDK tag
γ-tubulin

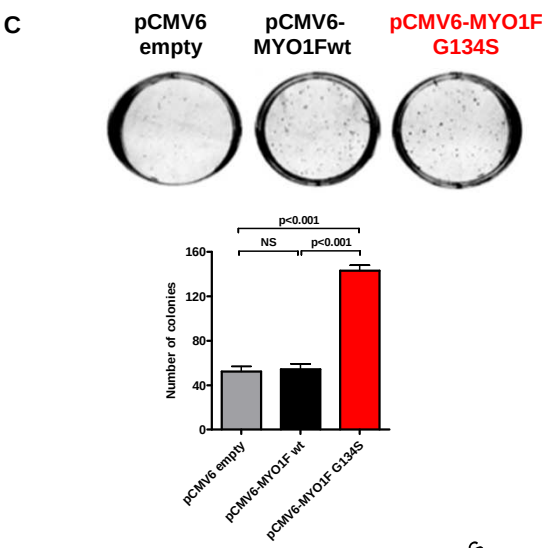
C
pCMV6 empty
pCMV6-MYO1Fwt
pCMV6-MYO1F G134S
p<0.001
NS
p<0.001
Number of colonies
0
40
80
120
160
pCMV6 empty
pCMV6-MYO1F wt
pCMV6-MYO1F G134S

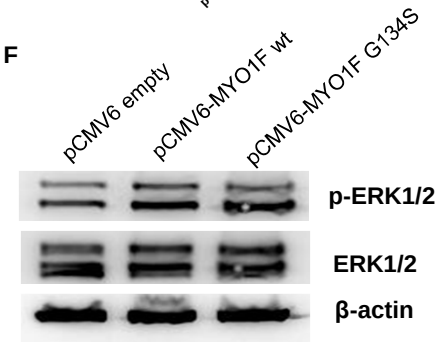
F
pCMV6 empty
pCMV6-MYO1F wt
pCMV6-MYO1F G134S
p-ERK1/2
ERK1/2
β-actin

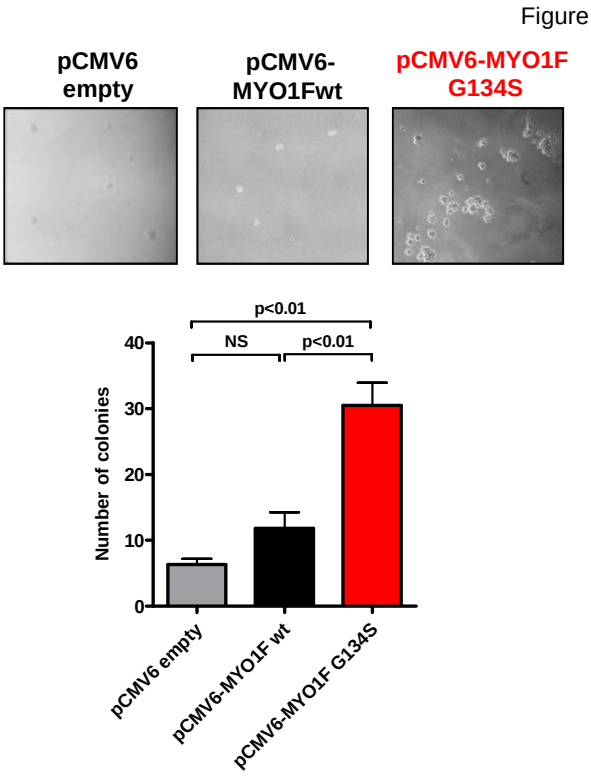
D
pCMV6 empty
pCMV6-MYO1Fwt
pCMV6-MYO1F G134S
p<0.01
NS
p<0.01
Number of colonies
0
10
20
30
40
pCMV6 empty
pCMV6-MYO1F wt
pCMV6-MYO1F G134S

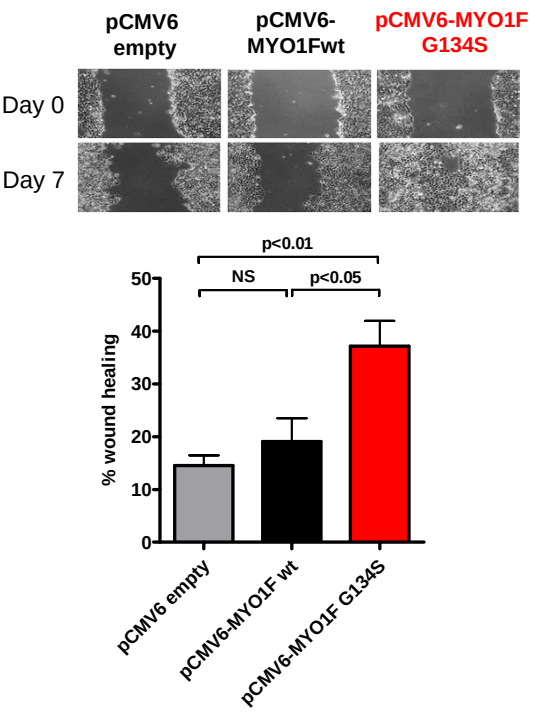
E
pCMV6 empty
pCMV6-MYO1Fwt
pCMV6-MYO1F G134S
Day 0
Day 7
p<0.01
NS
p<0.05
% wound healing
0
10
20
30
40
50
pCMV6 empty
pCMV6-MYO1F wt
pCMV6-MYO1F G134S

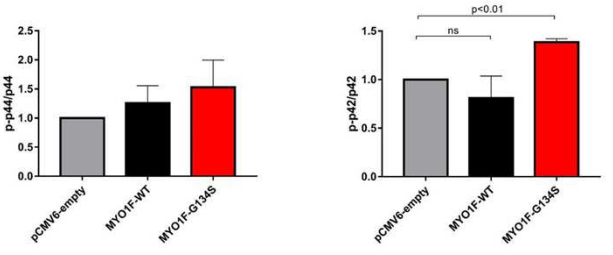
G
p-p44/p44
0.0
0.5
1.0
1.5
2.0
2.5
pCMV6-empty
MYO1F-WT
MYO1F-G134S
p<0.01
ns
p-p42/p42
0.0
0.5
1.0
1.5
pCMV6-empty
MYO1F-WT
MYO1F-G134S

Figure 2

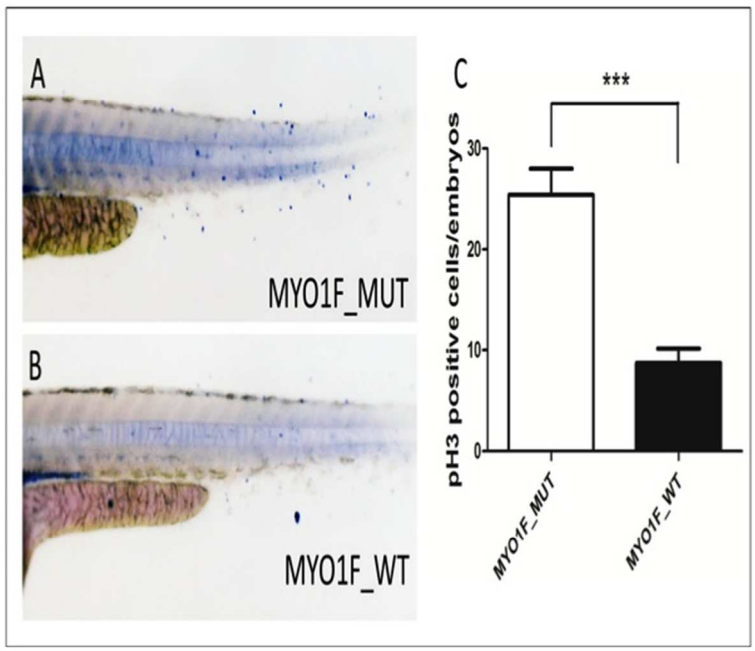

Proliferation analysis in zebrafish overexpressing either wild-type or mutant MYO1F p.134G>S: (A-B) Immunostaining of Phospho-histone H3 (pH3) performed in 48 hpf zebrafish larvae. An increase of cell proliferation can be observed in embryos injected with mutant MYO1F mRNA compared with embryos injected with the wild-type transcript of MYO1F. C) Quantification of pH3 -positive cells in injected embryos (48 hpf) was performed counting the number of mitotic cells along the trunk of each fish. For each group, 22 embryos were analyzed (MYO1F_MUT: 25.45 ± 2.584; MYO1F_WT: 8.727 ± 1.445). ***$P < 0.001$, Student's unpaired t-test.

254x338mm (72 x 72 DPI)

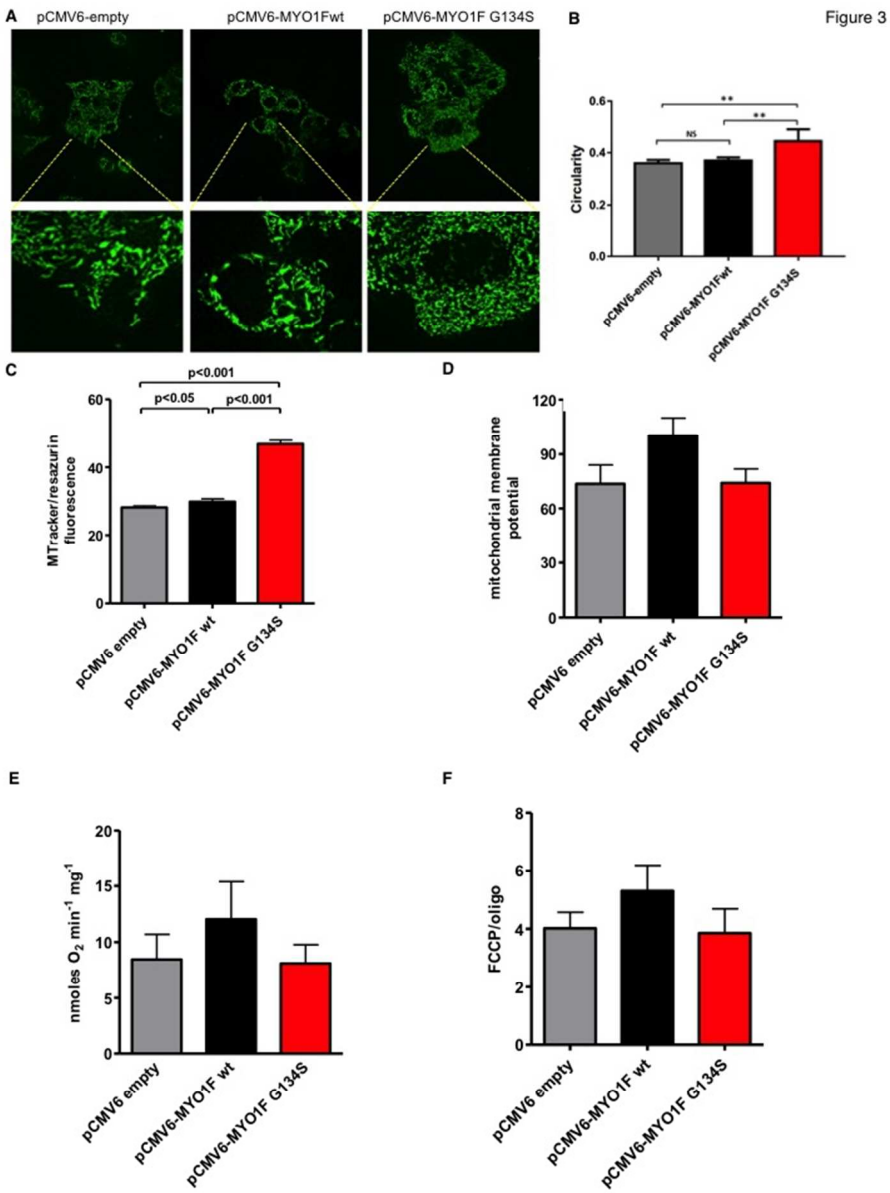

Mitochondrial defects in FRTL-5- MYO1F p.134G>S cells.
(A) Representative fluorescence images of pCMV6-empty, pCMV6-MYOF wild type and pCMV6-MYOF G134-S treated with Mitotracker Green to evaluate mitochondrial network. The cells expressing the mutant protein show more circular (B) and more abundant (C) mitochondria and more fragmented mitochondrial network in comparison with wild type and cells bearing empty vector. MitoTracker signal quantification was normalized on viable cell number assessed by resazurin-based assay. (D) To evaluate the mitochondrial membrane potential cells were treated with JC-1 fluorescent probe. In (D) the quantification of aggregate/monomer signal of JC-1 normalized on viable cell number is shown. Cell viability was assessed by resazurin-based method. (E) Basal rate of oxygen consumption in pCMV6-empty, pCMV6-MYOF wild type and pCMV6-MYOF G134>S cells. (F) shows the ratio between oxygen consumption in the presence of oligomycin and in the presence of FCCP (uncoupled respiration).

254x338mm (72 x 72 DPI)

Figure 4

A

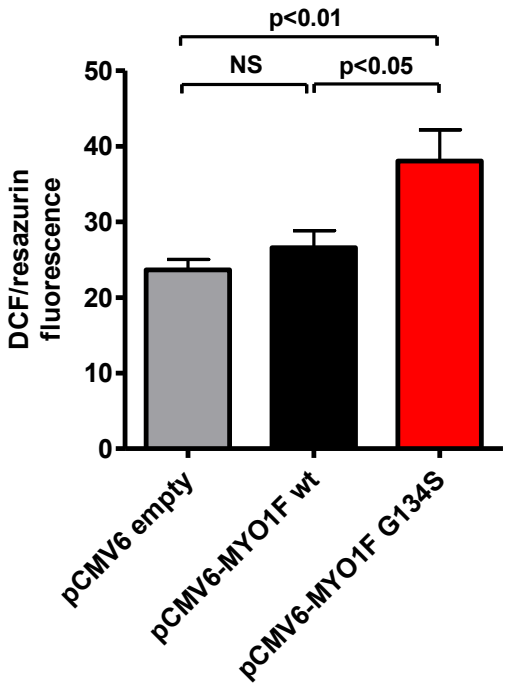
p<0.01
NS
p<0.05
DCF/resazurin fluorescence
50
40
30
20
10
0
pCMV6 empty
pCMV6-MYO1F wt
pCMV6-MYO1F G134S

B

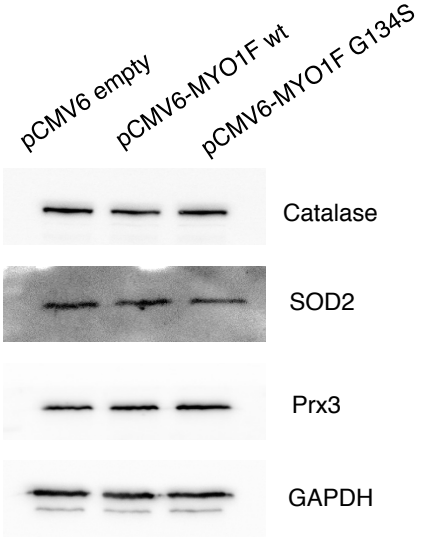
pCMV6 empty
pCMV6-MYO1F wt
pCMV6-MYO1F G134S
Catalase
SOD2
Prx3
GAPDH

C

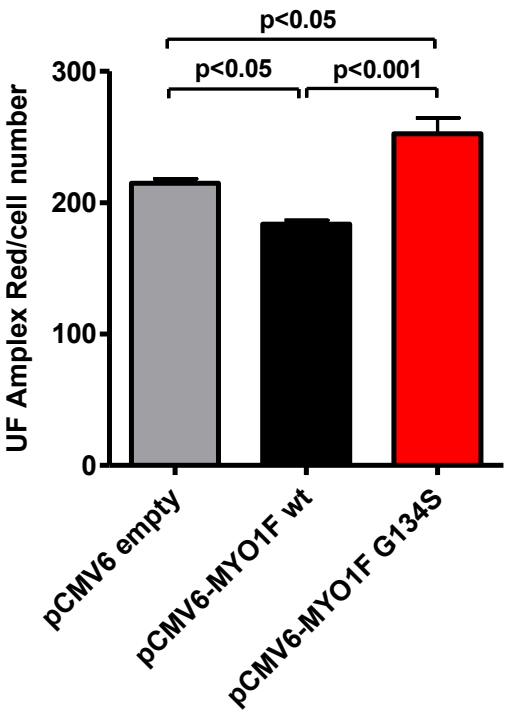
p<0.05
p<0.05
p<0.001
UF Amplex Red/cell number
300
200
100
0
pCMV6 empty
pCMV6-MYO1F wt
pCMV6-MYO1F G134S

Figure 5

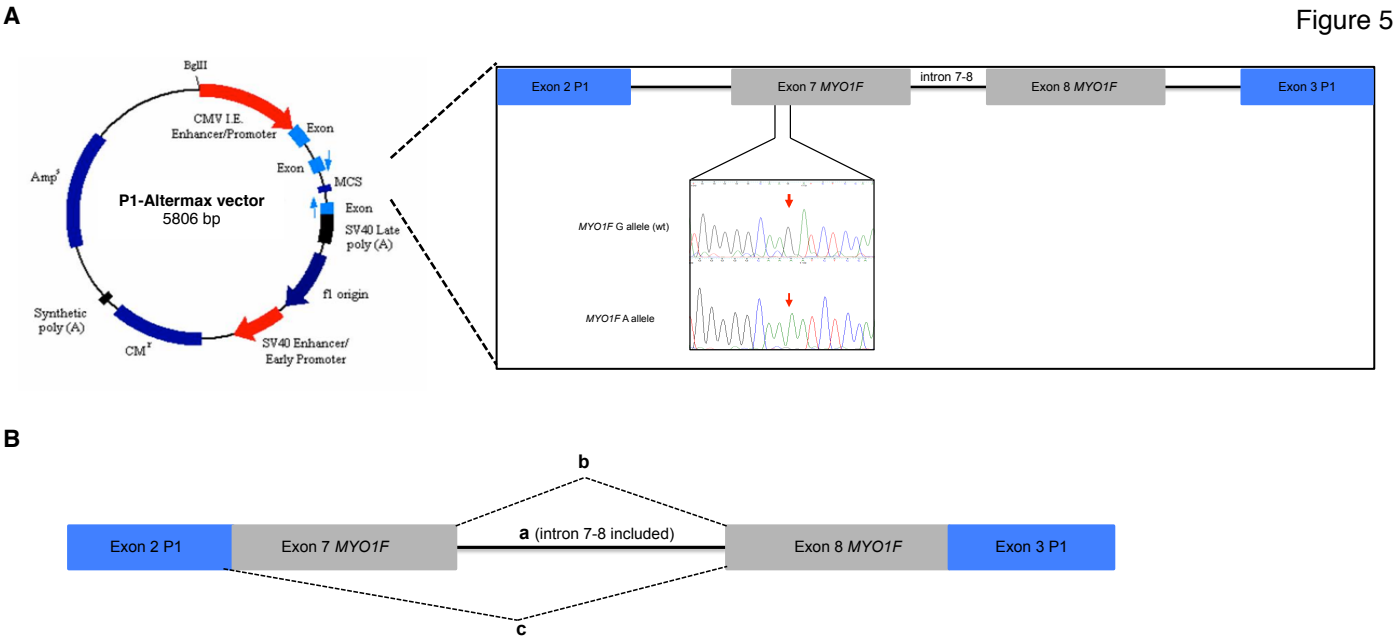
A
BglII
CMV I.E. Enhancer/Promoter
Exon
Exon
MCS
Exon
SV40 Late poly (A)
f1 origin
SV40 Enhancer/ Early Promoter
CM^r
Synthetic poly (A)
Amp^r
P1-Altermax vector
5806 bp
Exon 2 P1
Exon 7 MYO1F
intron 7-8
Exon 8 MYO1F
Exon 3 P1
MYO1F G allele (wt)
MYO1F A allele
B
b
Exon 2 P1
Exon 7 MYO1F
a (intron 7-8 included)
Exon 8 MYO1F
Exon 3 P1
c
C
M
untransfected COS7 cells
P1-empty vector
P1-MYO1F allele G (wt)
P1-MYO1F allele A
a
b
c
MYO1F Exon 7
Intron 7-8
MYO1F Exon 7
MYO1F Exon 8
Exon 2 P1
MYO1F Exon 8

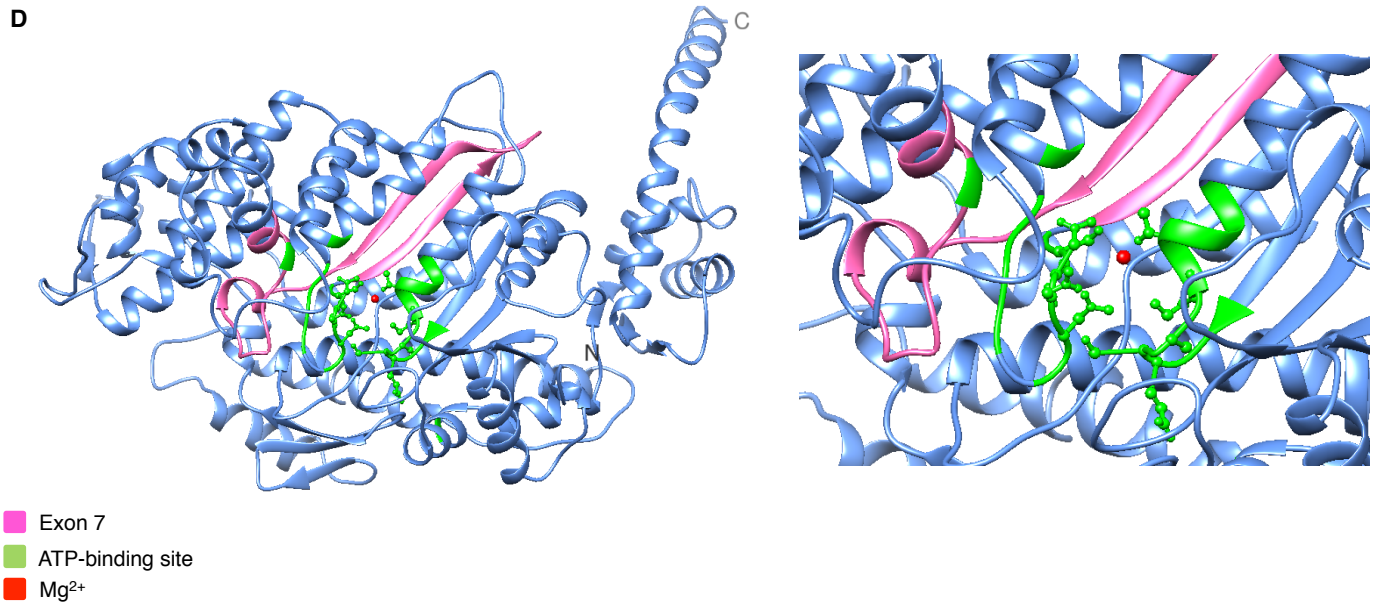
D
C
N
Exon 7
ATP-binding site
Mg2+